IOPscience iopscience.iop.org

Home Search Collections Journals About Contact us My IOPscience

In situ observation of size-scale effects on the mechanical properties of ZnO nanowires

This article has been downloaded from IOPscience. Please scroll down to see the full text article.

2011 Nanotechnology 22 265712

(http://iopscience.iop.org/0957-4484/22/26/265712)

View the table of contents for this issue, or go to the journal homepage for more

Download details:
IP Address: 71.13.213.8
The article was downloaded on 19/05/2011 at 03:47

Please note that terms and conditions apply.

Nanotechnology **22** (2011) 265712 (10pp) doi:10.1088/0957-4484/22/26/265712

In situ observation of size-scale effects on the mechanical properties of ZnO nanowires

A Asthana[1,3], K Momeni[1], A Prasad[2], Y K Yap[2,3] and R S Yassar[1,3]

[1] Department of Mechanical Engineering-Engineering Mechanics, Michigan Technological University, Houghton, MI 49931, USA
[2] Physics Department, Michigan Technological University, Houghton, MI 49931, USA

E-mail: aasthana@mtu.edu, ykyap@mtu.edu and reza@mtu.edu

Received 26 December 2010, in final form 20 April 2011
Published 18 May 2011
Online at stacks.iop.org/Nano/22/265712

Abstract

In this investigation, the size-scale in mechanical properties of individual [0001] ZnO nanowires and the correlation with atomic-scale arrangements were explored via *in situ* high-resolution transmission electron microscopy (TEM) equipped with atomic force microscopy (AFM) and nanoindentation (NI) systems. The Young's modulus was determined to be size-scale-dependent for nanowires with diameter, d, in the range of 40 nm $\leqslant d \leqslant$ 110 nm, and reached the maximum of ~249 GPa for $d = 40$ nm. However, this phenomenon was not observed for nanowires in the range of 200 nm $\leqslant d \leqslant$ 400 nm, where an average constant Young's modulus of ~147.3 GPa was detected, close to the modulus value of bulk ZnO. A size-scale dependence in the failure of nanowires was also observed. The thick ZnO nanowires ($d \geqslant$ 200 nm) were brittle, while the thin nanowires ($d \leqslant$ 110 nm) were highly flexible. The diameter effect and enhanced Young's modulus observed in thin ZnO nanowires are due to the combined effects of surface relaxation and long-range interactions present in ionic crystals, which leads to much stiffer surfaces than bulk wires. The brittle failure in thicker ZnO wires was initiated from the outermost layer, where the maximum tensile stress operates and propagates along the (0001) planes. After a number of loading and unloading cycles, the highly compressed region of the thinner nanowires was transformed from a crystalline to an amorphous phase, and the region near the neutral zone was converted into a mixture of disordered atomic planes and bent lattice fringes as revealed by high-resolution images.

1. Introduction

ZnO nanostructures have received increasing attention for various applications including nanoscale interconnects and active components in optical electronic devices and nano-electromechanical systems (NEMS). In addition, ZnO wires have a direct band gap of ~3.37 eV at room temperature, making them attractive wide band gap semiconductors for short wavelength light emitting devices and electron field emitters [1, 2]. ZnO has some extra advantages over other wide band gap materials. First, it exhibits both semiconducting and piezoelectric properties that can form the basis for electromechanically coupled sensors and transducers. Second, ZnO can be grown in a variety of nanostructures such as nanorings, nanobows, etc, which could be unique for many applications in nanotechnology [3].

The diameter dependent mechanical property of nanostructures was found to be important for application in NEMS and micromechanical systems [4]. The mechanical properties of individual ZnO nanostructures have been measured by various experimental techniques. The values of the elastic modulus reported so far range from 20 to 250 GPa [1, 5–9]. The wide range of values obtained is due to the different techniques of measurement and also due to the error associated with each technique. One of the initial nanomechanical testing techniques inside the transmission electron microscope was carried out by subjecting the nanowire/nanotube to

[3] Authors to whom any correspondence should be addressed.

 © 2011 IOP Publishing Ltd Printed in the UK & the USA

an alternating electrostatic field of known frequency and measuring the Young's modulus based on the dynamic response of the nanowire cantilever [4, 10, 11]. In a similar direction, Treacy *et al* [12] conducted the *in situ* measurement of the Young's modulus of a carbon nanotube in transmission electron microscopy (TEM) by increasing the specimen temperature and measuring the amplitude of its intrinsic thermal vibration. In these measurements, the deformation is gradient dominated and has a prominent surface elasticity effect [4]. Recently, several atomic force microscopy (AFM) based nanomechanical testing techniques have been developed. Although AFM-based techniques have sufficient force and displacement resolution, they are incapable of real-time imaging. Hence, the data interpretation is difficult and prone to measurement errors [13]. A nanoscale materials testing system consisting of a miniaturized testing stage based on MEMS (microelectromechanical system) technology has been developed recently [14–16]. Here, the load is applied using a thermal actuator on one side of the testing stage, and the displacement is measured using a differential capacitive sensor on the other side [17, 18]. The main difficulty in these systems is the complexity of their fabrication and tolerance variations in the fabricated devices. *In situ* AFM measurements inside TEM are among the new developments in the field of nanoscale mechanical testing systems. This technique allows one to perform mechanical measurements along with real-time imaging with a resolution close to 1 nN. In an *in situ* nanoindentation (NI) TEM system, the force data are read through a proper capacitive force sensor with the resolution close to 100 nN [19–21].

Here, we present a study on the *in situ* mechanical property measurement of individual thin ZnO nanowires (40 nm $\leqslant d \leqslant$ 110 nm) using an AFM–TEM system and that of thicker nanowires (200 nm $\leqslant d \leqslant$ 400 nm) by an NI–TEM system. This study was performed to better understand the effect of diameter scaling on the recorded mechanical properties of ZnO nanowires.

2. Experimental details

The system consists of an AFM/NI-equipped TEM sample holder, a controller, and a PC with Nanofactory's data acquisition software. All measurements were carried out on a single tilt AFM/NI holder in a JEM 4000FX TEM, operated at 200 keV. The setup of the AFM/TEM holder is shown in figure 1. The electrochemically etched gold wire with ZnO nanotubes (attached to the gold tip by conducting silver paste) was mounted to the piezo-driven movable part of the holder facing the fixed and sharp AFM/NI tip. The first step when using the AFM/NI–TEM setup is to calibrate the electrical conversion factor (C) of the force sensor. This constant is related to the electrical sensitivity of each sensor and must be set to a value that triggers a 1:1 correspondence of the F–d (force–displacement) relation when the cantilever is tested against the bare substrate of gold. In the present AFM system, $C = 10.1$ mV nm^{-1}, and for the NI system it is 1.01 pF/0.1 μN. In such an arrangement, atomic-scale imaging and F–d measurements are carried out concurrently.

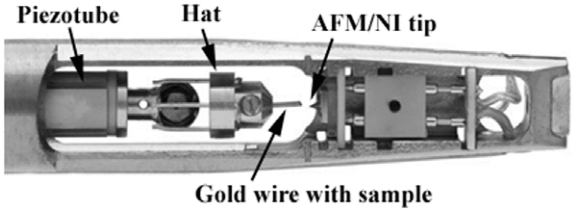

Figure 1. The *in situ* AFM/NI–TEM holder used for the present mechanical measurements.

The contact was made between the AFM/NI tip and the ZnO nanowire by the precision movement of the gold wire (with the sample) attached to the piezo-driven manipulator. To ensure the reliability of the recorded mechanical property data, it is important that the nanowires be firmly attached to the tip of the gold wire (250 μm diameter) mounted on the piezotube. To ensure this, the nanowires were attached to the gold substrate by silver paste. The contact at the tip end was achieved by sweeping a converged electron beam (probe diameter $\sim$ 30 nm) back and forth around the contact point of the nanowire to the NI/AFM tip. In this set-up, the full nanowire–contacts system may be regarded as having a pinned and clamped configuration. Our ZnO nanostructured samples were synthesized by the thermal chemical vapor deposition method, as reported elsewhere [22, 23].

3. Results and discussion

Figures 2(a)–(f) show a series of images acquired during the *in situ* nanomechanical testing of a ZnO nanowire 40 nm in diameter. Figure 2(a) shows the ZnO nanowire in contact with the AFM tip and attached firmly to the gold wire. The nanowire sample used in our study was a good quality single crystal, having a [0001] oriented wurtzite structure with lattice constants of $a = 0.325$ nm and $c = 0.520$ nm, as shown from the high-resolution image and diffraction pattern (figure 2(b)), and was typically between 4 and 10 μm long. Figure 2(c) displays the ZnO nanowire under the compressive/bending state by incremental movement of the piezo-driven gold tip against the AFM tip. As the ZnO wire was strained, a few regions on the nanowire showed local bright field contrast. The local changes observed in contrast may be related to atomic distortion resulting from stress concentration. Figures 2(d) and (e) show the nanowire under a highly bent condition. After unloading, it was found that the nanowire resumed its original form from the highly bent state (figure 2(f) is the relaxed state after unloading). Figure 2(g) displays the corresponding force–displacement (F–d) plot obtained for this nanowire. A drop in force at 100 nN indicates a structural instability in the bent nanowire.

To estimate the state of stress in this configuration, the thin ZnO nanowire was modeled with a finite element modeling (FEM) package (COMSOL 4.0) as an elastic beam. The nanowire was subjected to large deformation, assuming that the wire was fixed at one end and pinned at the other end. Tetrahedral elements were used for meshing. The free end of the cantilever was displaced by 150 nm toward the fixed end. To model buckling using FEM analysis, the symmetry

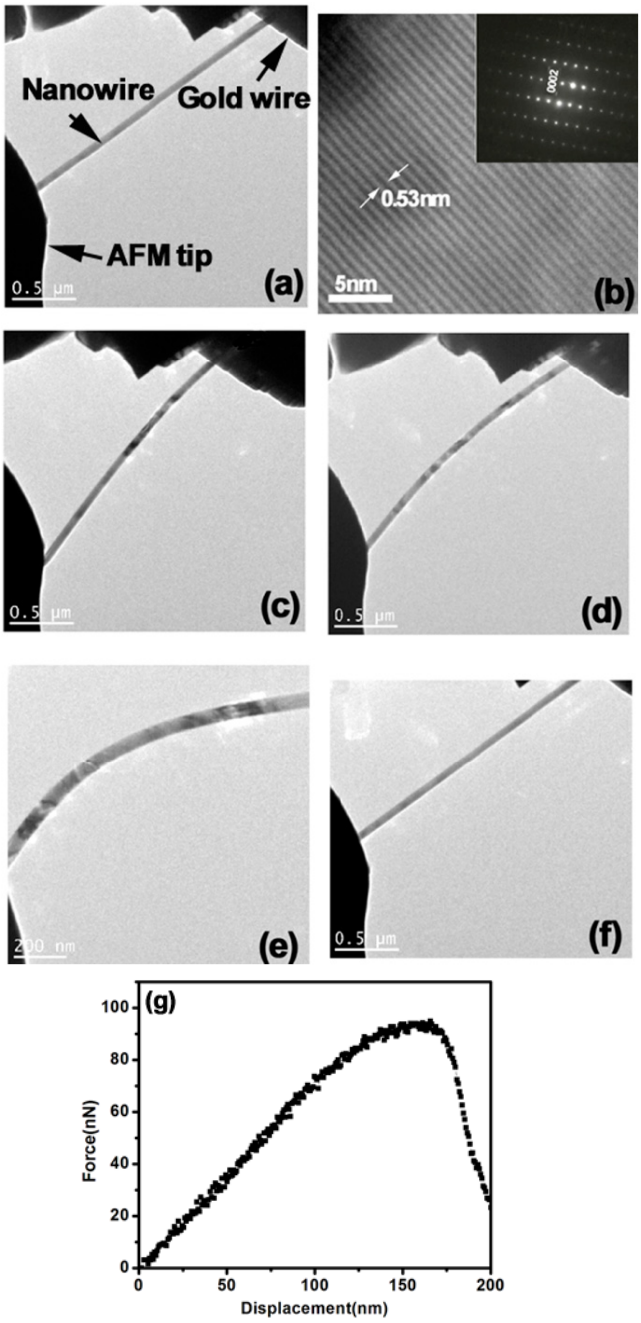

Figure 2. (a) The bright field image of a ZnO nanowire in contact with the AFM tip and attached firmly to the gold wire. (b) The high-resolution image and the corresponding diffraction pattern of the ZnO nanowire. (c)–(e) The nanowire under the axial force exerted by the incremental movement of the gold contact against the AFM tip. (f) The nanowire in relaxed state after unloading. (g) The corresponding force–displacement (F–d) plot where the maximum force corresponds to the buckling state of the nanowire.

of the problem had to be broken. This was done by upwardly displacing the free end by 50 nm. The FEM results in figure 3 show that the maximum deflection of the nanowire occurs in close approximately to its pinned end. This is consistent with the *in situ* TEM data. According to the FEM analysis, the maximum von Mises stress occurs at the fixed end and the highly deflected part of the nanowire.

The ZnO nanowires with a slenderness ratio (length/diameter) larger than 40 were regarded as long beams and, therefore Euler's buckling formula can be employed. In this scenario, the sudden force drop in figure 2(g) represents the Euler's buckling force, F_{Euler}. The Young's modulus of the nanowire can be estimated based on Euler's formula [24], $F_{\text{Euler}} = \frac{n\pi^2 EI}{L^2}$. Here, L is the length of the ZnO nanowire between the two contacts (=2.1 μm), E is the elastic modulus, and the moment of inertia is $I = 5\sqrt{3}a^4/16$ (considering the cross-section of the nanowire as a regular hexagon of side length a), determined from the bright field TEM image. The constant n is defined by a condition related to the end of the nanowire. The whole nanowire–contacts system may be regarded as having a pinned and clamped configuration. Hence, the value of n can be taken as ~0.707. Based on the above calculation, the Young's modulus for the nanowire of diameter 40 nm is estimated to be 249.3 (±1.8) GPa under the elastic limit. We tested several nanowires ranging from 110 to 40 nm and found that the estimated values of the Young's modulus range from 199.2 (±2.5) to 249.3 (±1.80) GPa. The value of elastic modulus obtained under the present investigation is higher than those reported previously for ZnO nanowires [4–8], for nearly the same width of nanowires. We could not bend this nanowire ($d = 40$ nm) to its failure point, as it was too flexible and resulted in the displacement of the nanowire from the pinned end.

The second part of our present investigation deals with the mechanical property measurement of thick nanowires with diameters in the range 200 nm $\leqslant d \leqslant$ 400 nm. Figures 4(a)–(c) show the sequential images of a thick ZnO nanowire undergoing a bending process to the failure point. Figure 4(a) is the bright field image showing a 300 nm wide ZnO nanowire (NW 1) in contact with the NI tip and attached firmly to the gold wire at the other end. Figure 4(b) shows a slightly bent nanowire under the applied compressive force. This geometry resembles a clamped cantilever subjected to a shear force at the free end. In practice, the nanowire tip was bent by the piezo-driven movement of the gold wire against the NI tip. During the bending process, the nanowire fractured in a brittle mode (figure 4(c)) at a critical force of ~250 μN (figure 4(d)), with a cleavage plane perpendicular to the nanowire axis, i.e. parallel to the (0001) planes. Figure 4(d) displays the recorded F–d plots corresponding to the maximum compressive force at the failure point of NW 1 (figure 4(c)). It appears from figure 4(c) that the NW 1 is broken from a location close to the free end, which can be puzzling at first sight. A correct analysis of the deformation behavior in NW 1 cannot be conducted unless the effect of NW 2 (figure 4(a)) is taken into account. This configuration is shown schematically in figures 5(a) and (b). NW 2 has almost the same diameter as NW 1 but is shorter in length. This nanowire (NW 2) is also firmly attached to the gold wire. Interestingly, the shorter nanowire (NW 2) acts as a pivot point for bending NW 1 (the black arrow in figure 5(b)), thus reducing its effective cantilever length to ~550 nm. The fracture is expected to initiate from the pivot point as this location carries the highest amount of stress, as shown by the modeling results (figure 5). The FEM result for this nanowire is shown in figure 5(c). As confirmed by the *in situ* TEM

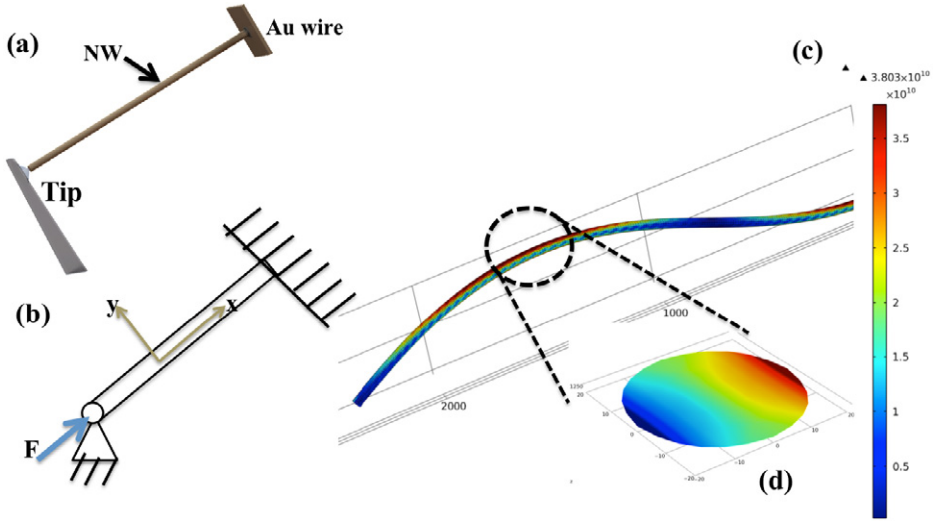

Figure 3. (a) Schematic of the thin ZnO nanowire configuration during deformation between the Au base and the AFM tip shown in figure 2. (b) The corresponding free-body diagram and the direction of applied force F on the nanowire. (c) The finite element simulation of the nanowire under the assumption of pinned and fixed configuration. (d) A 2D diagram corresponding to the von Mises stress at the highest displaced location along the length of the nanowire.

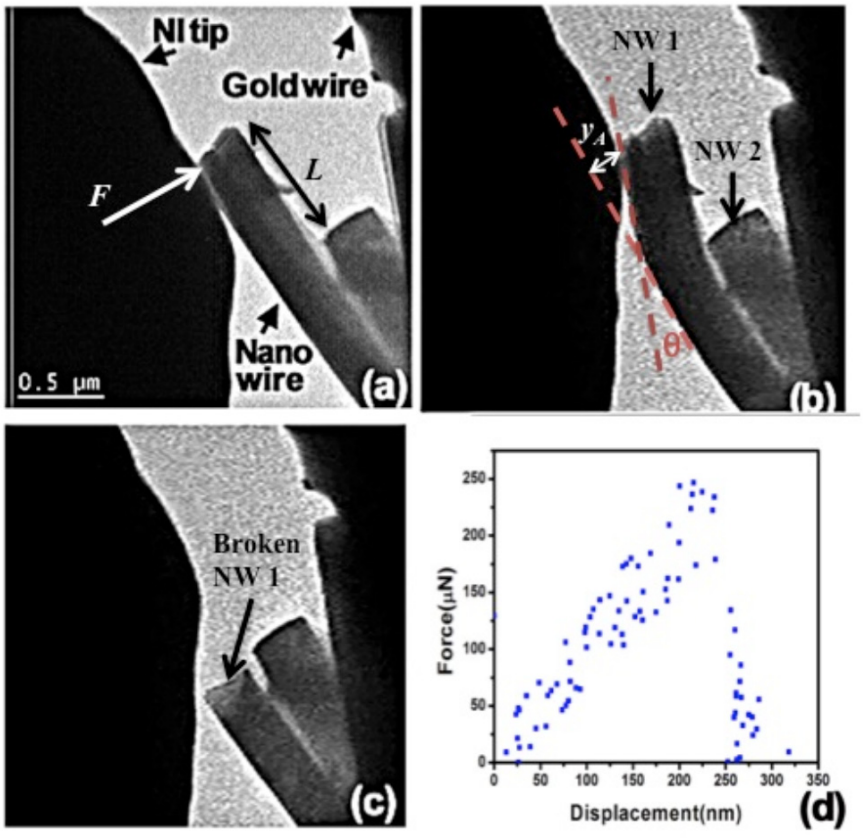

Figure 4. (a) The bright field image of a thick ZnO nanowire (∼300 nm) in contact with the NI tip and attached firmly to the gold wire at the other end. (b) A slightly bent nanowire under the applied compressive force. (c) An image of the broken nanowire. (d) The recorded F–d plot of this deformation behavior captures the failure point (maximum force) of the nanowire.

observation, the maximum deflection of the nanowire occurs at its free end. According to the FEM analysis, maximum von Mises stress occurs at the pivot point.

The Young's modulus can be obtained using the geometry of NW 1 at the maximum deflection illustrated in figure 4(b) and the maximum bending force. In general, for a cantilever under a bending force F (figure 5(d)), the curvature at any point (x, y) on the cantilever and the deflection y_A at the loading point $(L, 0)$ have well known relationships with the applied force F as $y_A = FL^3/3EI$ [25]. The diameter, d,

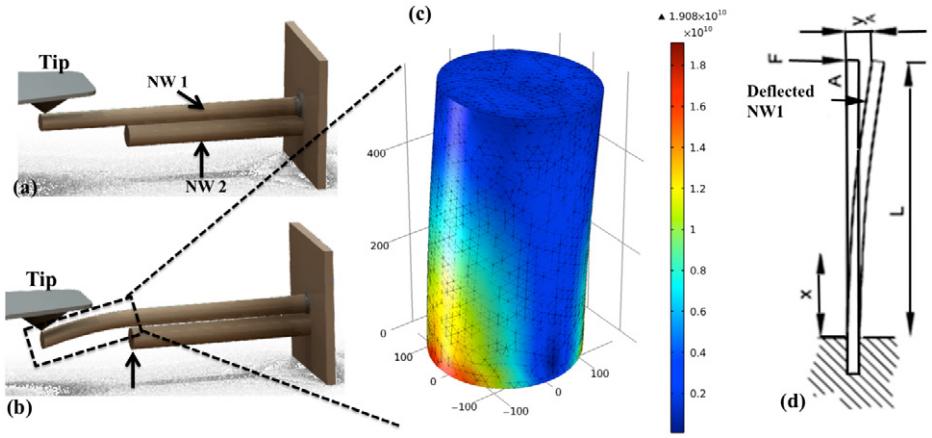

Figure 5. (a), (b) Schematics of the thick ZnO nanowire configuration during deformation between the Au base and the AFM tip shown in figure 4. (c) The corresponding von Mises stress obtained by finite element simulation of the nanowire under the fixed–free support assumption. (d) The corresponding free-body diagram shows that force F is being applied to the free end.

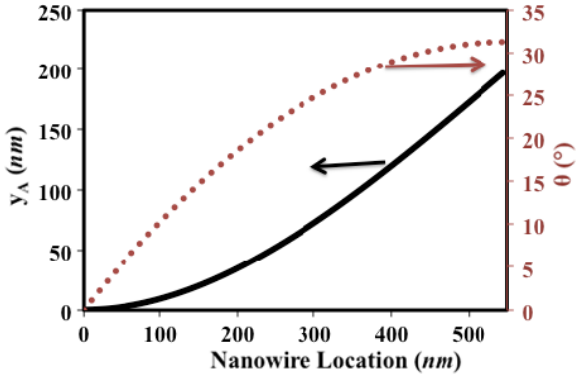

Figure 6. The bending angle θ (red dashed line), and the bending deflection y_A (black solid line) values plotted along the effective length of NW 1 (∼550 nm).

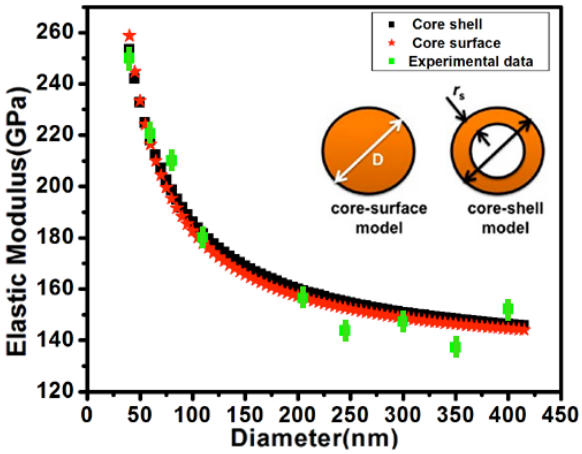

Figure 7. The variation of Young's modulus as a function of nanowire diameter. The fitting curves from the core–surface model (black) and the core–shell model (red) are also plotted. The inset shows the schematic of both models.

and the deflection, y_A, are determined from the bright field TEM image. Based on the above formula, the maximum elastic modulus for NW 1 was estimated to be 147.3 GPa. To check the accuracy of the adopted model, the bending angle, θ, and the bending deflection, y_A, values along the effective length of NW 1 (∼550 nm) were calculated and are plotted in figure 6. In particular, the predictions of deflection and bending values at the free end of NW 1 are in agreement with the bright field TEM observation shown in figure 4(b). The analysis of the above problem once again asserts that the *in situ* TEM observation can be invaluable to correctly interpret the experimentally recorded F–D data. For the nanowires with diameters in the range 200 nm $\leqslant d \leqslant$ 400 nm, the length of the nanowires was much shorter than for the thin nanowires ($L/d \leqslant 15$). Therefore, simple beam bending theories similar to the schematic in figure 5(d) were employed.

The calculated values of the Young's modulus as a function of wire diameter are plotted in figure 7. It is evident that the Young's modulus of [0001] oriented ZnO nanowires is diameter-dependent and varies sharply with diameters below 110 nm. For nanowires having diameter $d \geqslant$ 200 nm, the elastic modulus values were consistently between 130 and 155 GPa (figure 7). The estimated Young's modulus for ZnO nanowires with $d \geqslant$ 200 nm is close to the modulus values measured in bulk single crystals of ZnO (∼140 GPa) in the [0001] direction [26]. The synthesis of these nanowires was not different from that of the $d \leqslant$ 110 nanowires, which indicates that the Young's modulus property is affected by the size variations in the nanowires.

The observation of size-scale effects on the mechanical properties of ZnO nanowires is in agreement with the recent reported molecular dynamic (MD) simulations [18]. These simulations showed that the diameter scaling effect and higher value of Young's modulus for ZnO wires of diameters less than ∼100 nm are due to the surface reconstruction phenomenon. The effect of surface reconstruction is different in ZnO nanowire than in metallic nanowire [17, 27] due to the long-range ionic interaction in ZnO. The atomistic simulations predict that in ZnO nanowires, the surfaces are initially in a compression state, leading to the overall axial expansion of the nanowire upon relaxation. Due to the high radial

contraction of the surface, the surface atoms have smaller effective interatomic radii and hence the surface atoms exhibit a much higher elastic modulus compared to the inner atoms. It is expected that for very thin nanowires the contribution of the surface atoms to the overall elastic modulus dominates the behavior of the nanowire. However, this diameter scaling effect is less effective at larger diameters. Several other mechanisms have also been proposed to explain the observed size-scale effect in ZnO nanowires. Kulkarni *et al* [28] and Cao *et al* [29] reported that the nonlinear elastic response of the nanowire core (interior) is effective in determining the elastic modulus of the nanowire. In contrast, Zhang and Huang [30] found that due to increased electron density on the surface, there is saturation of the bond, and this is responsible for the stiffening of the nanowire as the size decreases.

In order to quantify the contribution of the surface and core elasticity of ZnO nanowires, the results were fitted into the core–surface model (or Miller–Shenoy model) [31] and the core–shell model [4]. The schematics of both models are shown in the inset of figure 7. The core–surface model is a continuum mechanics approach that embodies the surface effect [32–34]. The model essentially assumes that a nanowire consists of a core with elastic modulus E_c and a surface (zero thickness) with surface elastic modulus S (Pa m). Under bending, the measured (or effective) Young's modulus E is given by

$$E = E_c + 8\frac{S}{D}. \tag{1}$$

In the core–shell model, the nanowire consists of a core with elastic modulus E_c and a shell with elastic modulus E_s:

$$E = E_c\left[1 + 8\left(\frac{E_s}{E_c} - 1\right)\left(\frac{r_s}{D} - 3\frac{r_s^2}{D^2} + 4\frac{r_s^3}{D^3} - 2\frac{r_s^4}{D^4}\right)\right] \tag{2}$$

where D is the outer diameter of the circular cross-section and r_s is the shell thickness. Both models were fitted to our experimental data obtained from the bending of the nanowires following equations (1) and (2). In the core–surface model, it was found that the core elastic modulus $E_c = 131.9$ (± 4.3) GPa and the surface elastic modulus $S = 445.4$ (± 43.2) N m^{-1} and in the core–shell model $E_c = 127.2$ (± 4.3) GPa, and the shell elastic modulus $E_s = 372.1$ (± 14.2) GPa. The shell thickness r_s was chosen as 2.42 nm based on the recent report of Xu *et al* [35]. It appears that both models can predict the experimental data as evidenced in figure 7. However, it is observed that the estimated values of the core elastic modulus from both the models differ by approximately (5–10)% from the bulk value ($\sim$140 GPa), which may be indicative of surface stress [36].

After applying a number of loading and unloading cycles, no prominent change in internal structure was evident for the thin ZnO nanowires. This exceptionally high flexibility is unexpected due to the ionic nature of Zn^{2+} and O^{2-} bonding. During the buckling state shown in figures 8(a) and 9(a) (similar to figure 2(e)), we did not observe any breakage in the nanowire, except that diffraction contrast was prominent due to changes in the mass–thickness contrast. However, careful observation of the high-resolution image of the compressive region (marked by the framed square (I) in figure 9(a)) shows that the compressive-stressed region has transformed from crystalline to amorphous state while the crystalline order in the tensile region of the nanowire has changed only slightly.

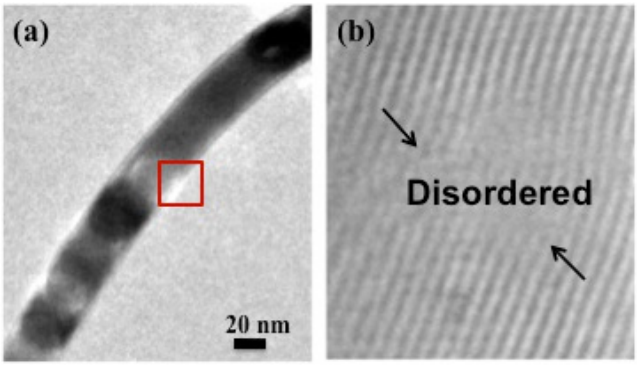

Figure 8. (a) Bright field TEM image of a thin ZnO nanowire in a bending state after four cycles of loading and unloading. (b) The high-resolution image of the marked region in (a) shows that there is breaking of the atomic lattice and disordering in the marked region. (This figure is in colour only in the electronic version)

In nanostructured materials the surface-to-volume ratio is high, hence there are large numbers of surface atoms that are not in equilibrium due to missing neighboring atoms at the surface. Statistically, these atoms have less constraint on movement in comparison to the core atoms. In a highly bending state where the surface atoms bear the maximum tensile and compressive stresses, disordering of atoms on the surface can occur. This might trigger the crystalline-to-amorphous transformation into an amorphous structure [37, 38]. Such crystalline-to-amorphous transitions have been predicted by MD simulations, although for smaller ZnO nanowires. Kulkarni *et al* [28] reported that crystalline ZnO nanowires with diameters less than 1 nm transformed into amorphous structures, while this phenomenon was not observed for thicker nanowires. This observation was also confirmed by Dai *et al* [38] where ZnO nanowires with lateral dimension of 0.7 nm were transformed from crystalline to amorphous structures. The MD simulation of the 1.6 nm ZnO nanowires shows that upon tensile stress and relaxation, the nanowire does not completely transform into an amorphous phase. Hence, the state of transformation into the complete amorphous state depends on the size of the nanowire. These MD simulations indicate the important role of surface stresses and, if combined with external applied loads, they might be more effective in driving the crystalline-to-amorphous phase transitions.

The amorphous-to-crystalline transition starts with the generation of atomic disordering and dislocation activities in the nanowire. Several reports have also documented the transformation of crystalline structures to an amorphous state under straining and dislocation activities [39–43]. Figure 8(a) shows the ZnO nanowire in a bending state after four cycles of loading and unloading. The high-resolution image of the marked region in figure 8(a) shows that there is breakage of the atomic lattice and disordering in the region marked (figure 8(b)). After repeated stress

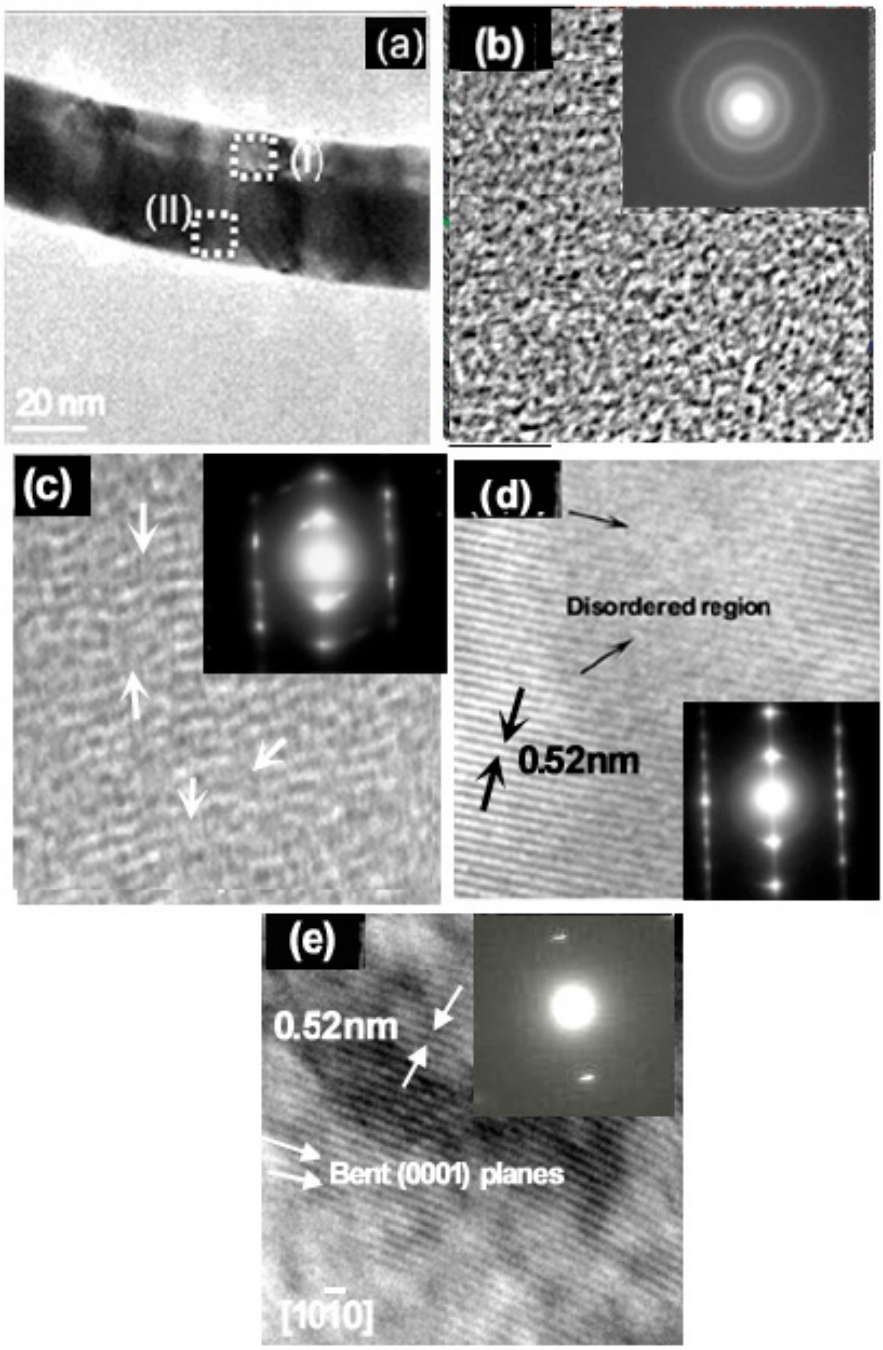

Figure 9. (a) A thin ZnO nanowire in bent condition is shown. The areas of interests marked as (I) and (II) were subjected to further analysis. (b) The high-resolution imaging and corresponding fuzzy diffraction pattern confirm the presence of the amorphous phase. (c) The high-resolution image shows the surrounding of the region (I). The corresponding diffraction pattern shown in the inset depicts the diffuse diffraction spot and streaks in the pattern indicating the presence of defects. (d) The tensile side, marked as region (II), shows a mixture of bending and breaking of the lattice image, indicating the generation of atomic disorder due to the high applied stress. The corresponding diffraction pattern from this region indicates the diffuse diffraction spots confirming the presence of defects. (e) The tensile-stressed region corresponding to the surrounding of region (II) on the neutral axis of the nanowire shows that the crystalline structure of the nanowire remains intact although there is slight bending of the (0001) lattice plane. The corresponding diffraction pattern shows slightly 'arc like' diffraction spots indicating bending lattice features.

cycles, the atomic disordering increases at the highly bent region, and some of these regions have transformed from a crystalline to an amorphous phase, as evidenced in figure 9. The high-resolution image of the region marked as (I) in figure 9(a) confirms the amorphous phase (figure 9(b)). The corresponding diffuse diffraction rings shown in the inset confirm the presence of amorphous regions. Figure 9(c) shows a high-resolution image of the surrounding region marked as (I). The image clearly shows the breaking of the lattice fringes due to the high dislocation density as marked by the

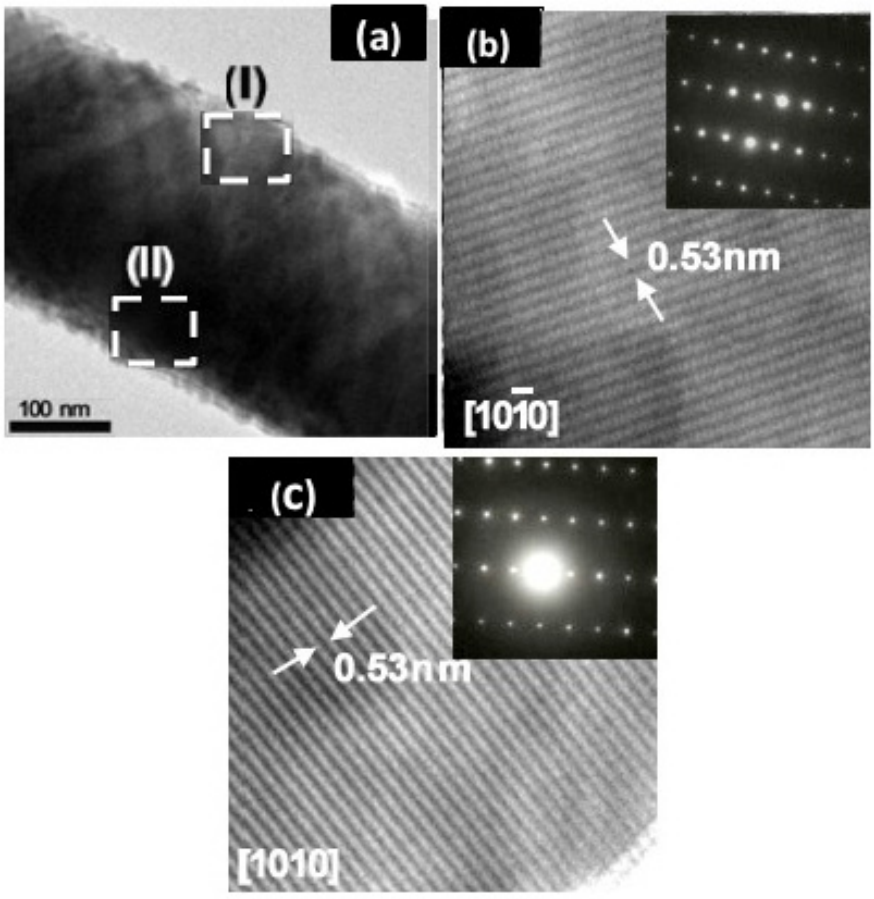

Figure 10. (a) A thick ZnO nanowire in bent condition is shown. The regions (I) and (II) were subjected to further examination. (b) The crystalline structure and corresponding diffraction of region (I). (c) The crystalline structure and corresponding diffraction of region (II). No indication of amorphous phase regions was observed.

white arrows. The corresponding diffraction pattern shown in the inset (figure 9(c)) depicts the diffuse diffraction spot and streaks in the pattern, indicating the presence of defects. The tensile side, marked as region (II), also shows the mixture of bending and breaking of the lattice image, indicating the generation of atomic disorder due to the high applied stress (figure 9(d)). The breaking of the lattice fringes shows that the dislocation line is moving along the (100) plane. The corresponding diffraction pattern (inset, figure 9(d)) from this region also shows the diffuse diffraction spots confirming the presence of defects. The tensile-stressed region corresponding to the surrounding region of the framed square (II) on the neutral axis of the nanowire shows that the crystalline structure of the nanowire remains intact although there is slight bending of the (0001) lattice plane with an estimated value of the lattice constant of ∼0.52 nm, corresponding to the *c* lattice constant of the wurtzite structure of ZnO (figure 9(e)). The corresponding diffraction pattern (inset, figure 9(e)) shows slight 'arc like' diffraction spots indicating bending lattice features [44]. The generation of such atomic disorders can lead to high flexibility in the nanowires as they impede the formation and progression of internal cracks. Our results and observations are in agreement with the recent report of Han *et al* [45] where the amorphization of a certain region for SiC nanowires under bending explained the observed large plasticity in the nanowires.

It is to be noted that we have observed the amorphous phase in the highly bent region of the ZnO thin nanowire after a number of cycles. We did not observe the formation of an amorphous phase on any other part of the nanotube, indicating that the amorphization of the highly bent part of the nanotube is not due to carbon contamination.

It should also be noted that the crystalline-to-amorphous transformation is more prone to forming in a compressive-stressed region compared to a tensile-stressed region. In the compressive-stressed region, an extra component of stress develops due to the formation of hoop stress. Hoop stress forms during the uniaxial compression of materials (not under tensile loading). This additional stress component increases the driving force for reconstruction of highly strained atoms in the compressed regions. However, the tensile-stressed region does not show the formation of the hoop stress, hence there is less driving force for atomic reconstruction in the tensile-stressed region as compared to the compressive-stressed region.

Interestingly, the thick nanowires (figure 10) did not show the generation of a detectable amorphous region, and the crystalline nature of the atomic structure in the bent region remained unchanged, as evidenced by the high-resolution images from regions (I) and (II) in figures 10(b)

and (c). The corresponding diffraction patterns (insets, figures 10(b) and (c)) show the sharp crystalline diffraction spots. The estimated value of the lattice fringe is ∼0.53 nm, corresponding to the *c* lattice constant of the wurtzite structure of ZnO. The ratio of surface atoms to core atoms decreases as the diameter of the nanowires increases. This will result in less contribution of the surface atoms on the governing properties of the nanowires. The surface atoms are not in a thermodynamic equilibrium state and, due to missing neighboring atoms, therefore have less constraint on movement or reorientation under applied stress. As such, due to a higher ratio of surface atoms in thin nanowires, there will be more chances for the nanoscale reconstruction of atoms (amorphous regions) under applied stress.

In the present investigations, the effect of the electron beam was minimized by conducting the structural characterization at a low beam current of 2.91 nA. The manipulation of the nanowires was done at a much lower beam current of 0.72 nA. The low beam currents of 0.72 and 2.91 nA were obtained by adjusting the possible combinations of condenser aperture and spot size. The electron beam was spread to avoid any convergence of the beam on the sample. In addition, we shut off the electron beam while recording the force–displacement data. Thus the related contamination and electron beam induced structural damage was minimized. Recent theoretical calculations show that the local temperature is no more than a few degrees above the room temperature under low beam currents [46]. In some of our previous work [47] the low current beam radiation did not induce any detectable change in the conductivity of the nanowires, indicating that the effect of the electron beam can be ignored in the analysis of the data presented in this work.

4. Conclusions

In conclusion, we utilized *in situ* TEM techniques to demonstrate the size-scale effect in the mechanical properties and flexibility of ZnO nanowires. Nanowires with diameters ranging from 40 nm $\leqslant d \leqslant$ 110 nm (thin nanowires) to 200 nm $\leqslant d \leqslant$ 400 nm (thick nanowires) were mechanically deformed using AFM and NI–TEM systems. Nanowires with 40 nm $\leqslant d \leqslant$ 110 nm exhibited strong size-scale effects, and the Young's modulus increased from 189.4 (±2.5) to 249.3 (±1.8) GPa as the wire diameter decreased from 110 to 40 nm. The dependence of the elastic modulus on the diameter was not observed for nanowires with 200 nm $\leqslant d \leqslant$ 400 nm. The values of Young's modulus in these nanowires varied between 130 and 155 GPa.

The diameter scaling effect and the higher value of Young's modulus observed in thinner ZnO nanowires (40 nm $\leqslant d \leqslant$ 110 nm) was due to the combined effects of surface relaxation and long-range interactions present in the ionic crystals, which led to much stiffer surfaces than the bulk. In the wires with diameters larger than 200 nm, the surface-to-volume ratio decreases and, hence, the surface stiffness effect also decreases. Therefore, the nanowire starts to exhibit the bulk behavior and brittle failure.

The high mechanical flexibility of the ZnO nanowires was associated with the crystalline-to-amorphous transitions. After a number of loading and unloading cycles, the highly deformed regions of the thin nanowires indicated local disordering and dislocation formation. The crystalline state of the thick nanowires remained intact during mechanical loading. To the authors' knowledge this is the first report on the observation of crystalline-to-amorphous transitions in ZnO nanowires.

Acknowledgments

The authors would like to acknowledge the funding support through the NSF-DMR grant no. 0820884 and NSF-CMMI grant no. 0926819.

References

[1] Muthukumar S, Shen H, Zhong J, Zhang Z, Emantoglu N W and Lu Y 2003 Selective MOCVD growth of ZnO nanotip *IEEE Trans. Nanotechnol.* **2** 50
[2] Look D C 2001 Recent advances in ZnO materials and devices *Mater. Sci. Eng.* B **80** 383
[3] Gao P X and Wang Z L 2005 Nanoarchitectures of semiconducting and piezoelectric zinc oxide *J. Appl. Phys.* **97** 044304
[4] Chen C Q, Shi Y, Zhang Y S, Zhu J and Yan Y J 2006 Size dependence of Young's modulus in ZnO nanowires *Phys. Rev. Lett.* **96** 075505
[5] Ni H and Li X 2006 Young's modulus of ZnO nanobelts measured using atomic force microscopy and nanoindentation techniques *Nanotechnology* **17** 3591
[6] Song J, Wang X, Riedo E and Wang Z L 2005 Elastic property of vertically aligned nanowires *Nano Lett.* **5** 1954
[7] Stan G, Ciobanu C V, Parthangal P M and Cook R F 2007 Diameter-dependent radial and tangential elastic moduli of ZnO nanowires *Nano Lett.* **7** 3691
[8] Simmons G and Wang H 1971 *Single Crystal Elastic Constants and Calculated Aggregate Properties* (Cambridge, MA: MIT Press)
[9] Yan X, Dickinson M, Schirer P J, Zou C and Gao W 2010 Face dependence of mechanical properties of a single ZnO nano/microrod *J. Appl. Phys.* **108** 056101
[10] Huang Y, Bai X and Zhang Y 2006 *In situ* mechanical properties of individual ZnO nanowires and the mass measurement of nanoparticles *J. Phys.: Condens. Matter* **18** L179
[11] Bai X D, Gao P X, Wang G L and Wang E G 2003 Dual-mode mechanical resonance of individual ZnO nanobelts *Appl. Phys. Lett.* **82** 4806
[12] Treacy M M J, Ebbesen T W and Gibson J M 1996 Exceptionally high Young's modulus observed for individual carbon nanotubes *Nature* **381** 678
[13] Agrawal R, Peng B, Gdoutos E E and Espinosa H D 2008 Elasticity size effects in ZnO nanowires—a combined experimental–computational approach *Nano Lett.* **8** 3668
[14] Zhu Y, Moldovan N and Espinosa H D 2005 A microelectromechanical load sensor for *in situ* electron and x-ray microscopy tensile testing of nanostructures *Appl. Phys. Lett.* **86** 013506
[15] Zhu Y and Espinosa H D 2005 An electromechanical material testing system for *in situ* electron microscopy and applications *Proc. Natl Acad. Sci. USA* **102** 14503
[16] Espinosa H D, Zhu Y and Moldovan N 2006 Design and operation of a MEMS-based material testing system for nanomechanical characterization *J. Micromech. Microeng.* **16** 242

[17] Diao J K, Gall K and Dunn M L 2003 Surface-stress-induced phase transformation in metal nanowires *Nat. Mater.* **2** 656
[18] Agrawal R, Peng B and Espinosa H D 2009 Experimental–computational investigation of ZnO nanowires strength and fracture *Nano Lett.* **9** 4177
[19] Wall M A and Dahmen U 1998 An *in situ* nanoindentation specimen holder for a high voltage transmission electron microscope *Microsc. Res. Technol.* **42** 248
[20] Stach E A *et al* 2001 Development of a nanoindenter for *in situ* transmission electron microscopy *Microsc. Microanal.* **7** 507
[21] Minor A M, Morris J W and Stach E A 2001 Quantitative *in situ* nanoindentation in an electron microscope *Appl. Phys. Lett.* **79** 1625
[22] Mensah S L, Kayastha V K, Ivanov I N, Geohegan D B and Yap Y K 2007 Formation of single crystalline ZnO nanotubes without catalysts and templates *Appl. Phys. Lett.* **90** 113108
[23] Mensah S L, Kayastha V K and Yap Y K 2007 Selective growth of pure and long ZnO nanowires by controlled vapor concentration gradients *J. Phys. Chem.* C **111** 16092
[24] Akita S, Nishijima H, Kishida T and Nakayama Y 2000 Influence of force acting on side face of carbon nanotube in atomic force microscopy *Japan. J. Appl. Phys.* **39** 3724
[25] Gere J M and Timoshenko S P 1984 *Mechanics of Materials* 2nd edn, vol 7 (Monterey, CA: Brooks/Cole) p 351
[26] Wen H 2004 *Single Crystal Elastic Constants and Calculated Bulk Properties* (Berlin: Logos)
[27] Diao J K, Gall K and Dunn M L 2004 Surface stress driven reorientation of gold nanowires *Phys. Rev.* B **70** 075413
[28] Kulkarni A J, Zhou M and Ke F J 2005 Orientation and size dependence of the elastic properties of zinc oxide nanobelts *Nanotechnology* **16** 2749
[29] Cao G X and Chen X 2007 Energy analysis of size-dependent elastic properties of ZnO nanofilms using atomistic simulations *Phys. Rev.* B **76** 165407
[30] Zhang L and Huang H C 2006 Young's moduli of ZnO nanoplates: *ab initio* determinations *Appl. Phys. Lett.* **89** 183111
[31] Miller R E and Shenoy V B 2000 Size-dependent elastic properties of nanosized structural elements *Nanotechnology* **11** 139
[32] Gurtin M E and Murdoch A I 1975 A continuum theory of elastic material surfaces *Arch. Ration. Mech. Anal.* **57** 291
[33] Cammarata R C 1994 Surface and interface stress effects on interfacial and nanostructured materials *Prog. Surf. Sci.* **46** 1
[34] Gibbs J W 1906 *The Scientific papers of J Willard Gibbs* vol 1 (London: Longmans Green) p 55
[35] Xu F, Qin Q, Mishra A and Gu Y 2010 Mechanical properties of ZnO nanowires under different loading modes *Nano Res.* **3** 271
[36] He M R, Shi Y, Zhou W, Chen J W, Yan Y J and Zhu J 2009 Diameter dependence of modulus in zinc oxide nanowires and the effect of loading mode: *in situ* experiments and universal core–shell approach *Appl. Phys. Lett.* **95** 091912
[37] Gumbsch P, Riedle J, Hartmaier A and Fischmeister H F 1998 Controlling factors for the brittle-to-ductile transition in tungsten single crystals *Science* **282** 1293
[38] Dai L, Sow C H, Lim C T, Cheong W C D and Tan V B C 2009 Numerical investigations into the tensile behavior of TiO_2 nanowires: structural deformation, mechanical properties, and size effects *Nano Lett.* **9** 576–82
[39] Koike J, Parkin D M and Nastasi M 1990 Crystal-to-amorphous transformation of NiTi induced by old rolling *J. Mater. Res.* **5** 1414
[40] Antonov V E, Barkalov O I and Ponyatovsky E G 1996 Crystal-to-amorphous phase transformation of the Ga–Sb high-pressure phase *J. Non-Cryst. Solids* **192** 443
[41] Tsuchiya K, Waitz T, Hara T, Karnthaler H P, Todaka Y and Umemoto M 2008 Crystalline-to-amorphous transformation in intermetallic compounds by severe plastic deformation *EMC 2008: 14th Electron Microscopy Congress (Aachen, Sept. 2008)* pp 385–6
[42] Branicio P S and Rino J P 2000 Large deformation and amorphization of Ni nanowires under uniaxial strain: a molecular dynamics study *Phys. Rev.* B **62** 16950
[43] Ikeda H 1999 Strain rate induced amorphization in metallic nanowires *Phys. Rev. Lett.* **82** 2900
[44] Asthana A, Matsui Y, Yasuda M, Kimoto K, Iwata T and Ohshima K 2005 Investigations on the structural disordering of neutron-irradiated highly oriented pyrolytic graphite by x-ray diffraction and electron microscopy *J. Appl. Crystallogr.* **38** 361
[45] Han X D, Zhang Y F, Zheng K, Zhang X N, Zhang Z, Hao Y J, Guo X Y, Yuan J and Wang Z L 2007 Low-temperature *in situ* large strain plasticity of ceramic SiC nanowires and its atomic-scale mechanism *Nano Lett.* **7** 452
[46] Jencic I, Bench M W, Robertson I M and Kirk M A 1995 Electron beam induced crystallization of isolated amorphous regions in Si, Ge, GaP and GaAs *J. Appl. Phys.* **78** 974
[47] Asthana A, Momeni K, Yassar R S, Prasad A and Yap Y K 2009 *In situ* probing of electromechanical properties of an individual ZnO nanobelt *Appl. Phys. Lett.* **95** 172106